Repeated Impacts Tests and Nanoindentation as Complementary Tools for Mechanical Characterization of Polymer-Coated Particles

G. Perfetti,[1] J. Arfsten,[2] A. Kwade,[2] W. J. Wildeboer,[3] G. M. H. Meesters[1,3]

[1]*DelftChemTech DCT, Nanostructured Materials Group NSM, Faculty of Applied Sciences, Delft University of Technology, 2628 BL Delft, Netherlands*
[2]*Institute for Particle Technology, Technische Universität Braunschweig, Braunschweig 38104, Germany*
[3]*DSM Food Specialties, P.O. Box 1, Delft 2600, MA, Netherlands*

Received 21 April 2009; accepted 30 January 2010
DOI 10.1002/app.32215
Published online 26 May 2010 in Wiley InterScience (www.interscience.wiley.com).

ABSTRACT: Polymer-coated particles have been produced by applying two grades of hydroxypropyl methylcellulose and one grade of polyvinyl alcohol onto sodium benzoate Purox-S core particles by using top-spray fluid bed coater and then stored under two different conditions, namely ambient conditions (23°C, 55% RH) and in the freezer (−18°C, 25% RH). Surface morphology has been firstly analyzed using scanning electron microscope and atomic force microscope. Resistance to attrition and viscoelastic properties have been measured by repeated impact tester (RIT) and nanoindentation, respectively. The resistance to attrition have been discussed as function of type of coating materials, breakage mechanisms, and storage temperature, and then compared with uncoated Purox-S. The storage conditions is not influencing the morphology, whereas is strongly affecting the resistance to attrition. Coated particles stored at −18°C were found to be more resistant to attrition than ones stored at room conditions. Such differences negligible at low energies (low numbers of impacts) increase as soon as the number of impacts and the energy rise. The improvement in the resistance to attrition was related to the plasticizing effect of water content. Displacement, storage modulus (E'), loss modulus (E''), and damping factor (tan δ) have been measured for all coated particles. Quasistatic and dynamic nanoindentation were found to agree very well with each other. Comparison of the nanoindentation results and the RIT results showed that tan δ, as measure of viscoelasticity and flexibility of the polymeric coating material, is related to the attrition behavior. It was found, in fact, that a higher tan δ gives more resistance to attrition. J Appl Polym Sci 118: 790–804, 2010

Key words: polymer coating; indentation; impact resistance; coating morphology; viscoelastic properties

INTRODUCTION

Nowadays, many particulate products are coated to give the product specific functionalities. Examples of these products are agglomerates, granules, tablets, pellets, and crystals in the chemical, pharmaceutical, and food industry. Possible reasons for applying coatings are[1]:

- Shelf life enhancement and prolongation, and to increase strength of the product to prevent dust formation.
- To improve processability and physical properties, such as solubility, dispersibility, hygroscopicity, and flowability, or to modify the density[2,3] and prevent segregation as well as to improve aesthetic-like color and the appearance of the company logo.
- To achieve controlled, sustained, delayed, and/or targeted drug delivery release properties.[4,5]
- Safe and convenient handling of toxic materials.
- To mask undesirable flavors or odors of the product.[6]
- To enhance the overall quality of food and pharmaceutical ingredients[7–11] and to stabilize ingredients during processing (e.g., heat, pressure, and moisture).
- To avoid caking during storage and facilitate dosage and mixing of the products.[12]
- To separate core unstable ingredients from their environment and prevent degradation reactions (e.g., moisture, acid, oxygen, high temperatures, light, or other food ingredients).[13,14]

A fundamental analysis of the coating material properties is required to ensure that the coated particles can withstand the mechanical stresses they are subjected to production, transportation, and

Correspondence to: G. Perfetti (g.perfetti@tudelft.nl).

handling. A coating shell with low mechanical strength may break during transport, leading to a change in the properties of the product. Storage conditions can also play an important role in preserving the properties of the coated particles. A lot of effort is devoted to the development of measuring systems that give a representative measure for coating shell resistance strength.[15] Among all these systems, repeated impact tester (RIT)[16,17] allows the measure of resistance to attrition.[17] Currently, the technology for preserving/enhancing the mechanical strength of coated particles mainly relies on experience. In fact, despite a large availability of data regarding the breakage resistance of coated particles, only little fundamental knowledge of coating shell strength and breakage has been obtained.

Therefore, in an engineering approach, a more extensive understanding of the intrinsic material properties of the coating agent is necessary to point out what characteristics are critical to resistance to attrition. The article presents nanoindentation, allowing the investigation of single layer polymer-coated particles produced by fluidized bed independently to core particle, as powerful tool for analysis and characterization of viscoelastic properties of coating shell, and thus, to explain the resistance to attrition. The main aim of this article is to proof that an exhaustive intrinsic characterization of the polymer coating shell itself obtained by nanoindentation is necessary when trying to explain the resistance to attrition (and breakage resistance in general) of the entire polymer-coated particles. The attrition behavior is measured with a RIT developed at Delft University of Technology.[16] The mechanical behavior of the coating layer is characterized by quasistatic and dynamic nanoindentation experiments. Viscoelastic material parameters (e.g. the storage and loss modulus) of the coating layers are extracted and discussed in respect of resistance to attrition.

In addition, a complete morphological characterization of the coated particles was conducted by means of scanning electron microscope (SEM) as well as atomic force microscope (AFM) and presented.

Repeated impact testing

Beekman et al.[16] designed a device for measuring the resistance of particles to attrition under repeated impacts. The technique was further developed by Pitchumani et al.[17]

The RIT accelerates particles towards the target and permits repeated impacts. There are two impacts for each turn of the flywheel. The particles are contained within the particle chamber and undergo impacts in unidirectional movement.[17] The impacts are mainly against the inner surfaces of the top and bottom wall of the chamber. Attrition is therefore dominating the mechanical stresses exerted onto the particles. Beekman[16] described three attrition submechanisms, which are peeling, erosion, and layer fatigue. The peeling mechanism, which we refer to as surface rounding, is characterized by initial removal of the corners, sharp edges, and outer layer of the particle. Once this layer is removed, the attrition rate decreases. Peeling is often followed by erosion, which is characterized by the linear decay of mass during attrition testing. The fatigue mechanism is the result of the accumulation of small damages, microcracks, and plastic deformation, without any visible effect on the particle at low energy until a collapsing point occurs. If layer fatigue is a dominant mechanism, initially no attrition is observed. The principles of the mechanisms and the typical shape of the graphs are described in Figure 1(b).

The impact velocity between the particles and the chamber is equal to the maximal chamber velocity, which can be calculated by eq. (1).

$$v_p = 2\pi fA \tag{1}$$

where f is the oscillation frequency of the flywheel and A is the amplitude of the motion of the chamber, which is constant and equal to the radius of the flywheel. The number of impacts (N) can be calculated using eq. (2):

$$N = 2ft \tag{2}$$

where t is the total duration of the experiment and f is the frequency of the flywheel. The resistance to attrition is quantified by the analysis of the fraction of undamaged particles as function of impact energy, which is proportional to the number of impacts. The particles were weighed before and after the RIT to determine the remaining mass (m_{rm}) using eq. (3):

$$m_{rm} = \frac{m}{m_0} \tag{3}$$

where m is the mass of intact particles after the RIT experiment and m_0 is the initial particle mass. The measurement error in the balance is in the order of 0.07%.[18] The mass specific energy of impact ($E_{i,m}$) expressed in J/kg, representing the total amount of energy transferred, effectively stored in the particles and responsible of the breakage of the particles is a fraction of the mass specific kinetic energy ($E_{k,m}$) and can be calculated using eq. (4).

$$E_{i,m} = E_{k,m}(1-e) = \frac{1}{2} m_{rm} {v_p}^2 (1-e)N \tag{4}$$

where e is the coefficient of restitution of the particles and $(1-e)$ is then the fraction of $E_{k,m}$ stored in

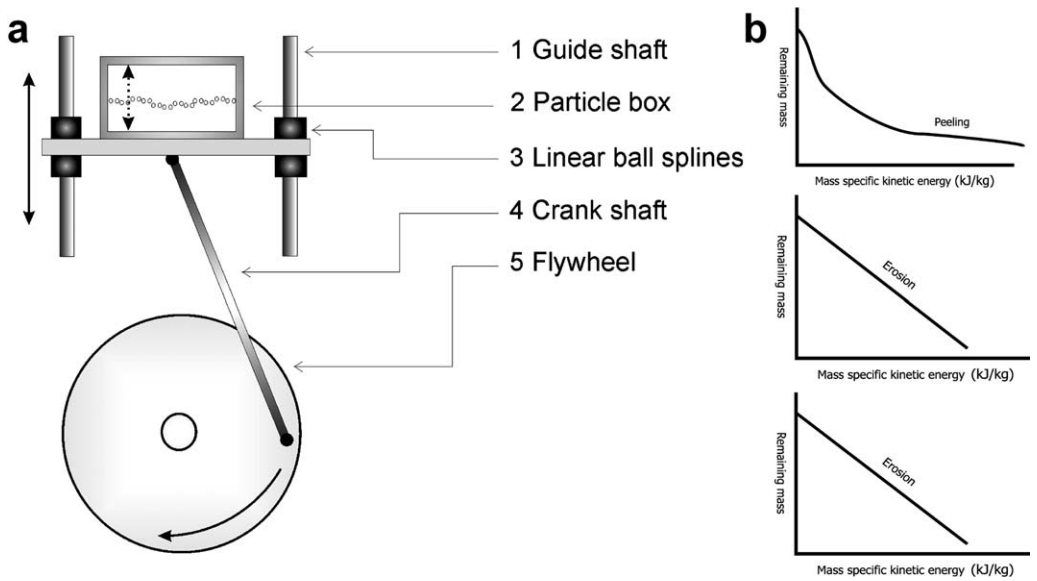

Figure 1 Schematic drawing of the repeated impact tester (RIT) (a) and attrition mechanisms as proposed by Beekman[16] (b).

the particle after the impact as strain energy, microcracks or local plastic deformation, $E_{k,m}$ the mass specific kinetic energy in (J/kg), m_{rm} the resulting normalized remaining mass after experiment, v_p the particle impact velocity as calculated by eq. (1) and N the number of impacts.

A more detailed description of the measurement device was given by Pitchumani et al.[17]

Nanoindentation

Nanoindentation, also known as instrumented indentation or depth-sensing indentation, is increasingly applied to study the mechanical behavior of materials. The technique was derived from traditional hardness testing (e.g., Vickers or Rockwell hardness testing). A diamond with a specific tip shape is pressed into the material of interest. The forces involved are commonly in the μN–mN range and the indentation depths are usually in the order of nanometer to micrometer.[19] A force-displacement curve is recorded, which is translated into mechanical parameters. The Oliver–Pharr method[20] is a commonly used and reliable method to determine the hardness and Youngs's modulus of a flat elastic-plastic sample from the nanoindentation load-displacement data. Over the past 20 years, nanoindentation has become a routinely used technique to study the mechanical properties of materials, such as metals or ceramics.[21–23]

However, measuring polymeric materials and the extraction of meaningful mechanical parameters is much more challenging because of the softness and the time-dependent behavior of those materials. For these materials, the shape of the force-displacement curve is strongly influenced by the indentation speed. Thus, a dynamic nanoindentation technique should be applied. During a dynamic nanoindentation test a sinusoidal load with preset load amplitude F_0 and preset frequency ω is imposed on the sample during the indentation procedure. Using a lock-in-amplifier, the resulting displacement amplitude X and the phase shift ϕ of the signal is measured at the same frequency. Hereby, the contact for the dynamic test is modeled by a single degree of freedom, damped and forced harmonic oscillator.

A linear viscoelastic material is commonly described by a spring (spring stiffness, S) and a dashpot (damping coefficient, D) in parallel (Voigt model). The portion of the displacement response, that is, in phase with the imposed load (elastic portion) allows the determination of S:

$$S = \frac{F_0}{X}\frac{1}{\sqrt{1+\tan^2\phi}} + m\omega^2 \tag{5}$$

where, S is proportional to the ratio of the applied force amplitude to the displacement amplitude, that is, in phase with the applied force, m is the mass of the sensor, ϕ the phase shift, ω the preset frequency, F_0 the preset load amplitude and X the resulting displacement amplitude of the dynamic indentation.

The out-of-phase response that reflects the energy absorbed by the material can be used to determine the damping coefficient D:

TABLE I
Details on Pharmacoat® 603 (HPMC 603), Pharmacoat® 615 (HPMC 615), and Mowiol® 4–98, (PVA 4–98)

Polymer	Brand name	Grade	Degrees of substitution [% w /w]		M_w	Viscosity[a] [Pa s]	Hydrolysis (Mol %)
			Methoxy	Hydroxypropoxyl			
Hydroxypropyl Methylcellulose	Pharmacoat	603[a]	28.0– 30.0	7.0– 2.0	13000	4.5–5	
	Pharmacoat	615[b]	28.0–30.0	7.0–12.0	65000	29–31	
Polyvinyl alcohol	Mowiol	4–98[c]			27000	4–4.5	98–98.8

[a] 3% solution in water at 25 °C.[35]
[a] T_g = 151.3°C (DMTA; cast films from 3% w/w aqueous solution).[35]
[b] T_g = 165.5°C (DMTA; cast films from 3% w/w aqueous solution).[35]
[c] T_g = 33°C (DMTA; cast films from 3% w/w aqueous solution).[35]

$$D = \sqrt{\frac{(\frac{F_0}{X})^2 \tan^2\phi}{1+\tan^2\phi}}\left(\frac{1}{\omega}\right) \quad (6)$$

Combination of dynamic material's response with elastic contact theory allows the determination of the storage modulus, E', (characterizes the elastic behavior of the material) and the loss modulus, E'', (characteristic for the internal damping) of the material:

$$E' = \frac{S\sqrt{\pi}}{2\sqrt{A_c}} \quad (7)$$

$$E'' = \frac{\omega D\sqrt{\pi}}{2\sqrt{A_c}} \quad (8)$$

where A_c is the projected contact area, which is obtained from the calibrated tip-area-function (relationship between the projected contact area of the indenter tip and the contact depth).

The loss tangent (tan δ) is defined as the ratio of E'' to E', and therefore, as the ratio of dissipated to stored energy:

$$\tan\delta = \frac{E''}{E'} = \frac{D\omega}{S} \quad (9)$$

In contrast to E' and E'', tan δ does not depend on the projected contact area A_c, which determination is often connected with uncertainties. Therefore, tan δ is a more robust parameter for the description of viscoelastic material behavior than E' and E''.[24]

A more detailed description of the dynamic nanoindenation procedure as well as the corresponding data analysis can be found elsewhere.[19,25,26]

Dynamic nanoindentation was first applied to polymers in 1995 by Loubet et al.[27] Several studies on dynamic viscoelastic characterization of polymers have been performed since then.[24–31] Nevertheless, quasistatic indentation is still used more frequently than dynamic nanoindentation. There are no standard methods to perform dynamic nanoindentation, e.g., how to determine a suitable frequency and amplitude, and there is no common procedure to process the measurement data. Even though further improvements in measurement procedure and data analysis are necessary, dynamic nanoindentation has already proven to be a very suitable method to detect differences in the mechanical behavior of different materials, especially polymeric materials.[32–34]

MATERIALS AND METHODS

Materials

Polymer-coated sodium benzoate particles were chosen as a model system for this work. The sodium benzoate, Purox-S®, was supplied by DSM, Geleen, The Netherlands.

The particle size was in the range of 1000–1300 μm and the particles were spherical with some sharp edges. Aqueous polymer solutions were used as coating agents. The following materials were used: (1) two grades of highly substituted hydroxypropyl methylcelluloses (HPMCs), Pharmacoat® 603 and Pharmacoat® 615, supplied by Syntapharm, Mülheim an der Ruhr, Germany (referred to as HPMC 603 and HPMC 615, respectively, further in this article), and (2) one grade of polyvinyl alcohol (PVA) Mowiol® 4–98, supplied by Sigma-Aldrich, UK (referred to as PVA 4–98 further in this article). All the polymers were used without any pretreatment (Table I).

Coating procedure

Preparation of Solutions

Both HPMC and PVA aqueous solutions were prepared at 3% w/w. HPMC was dispersed and dissolved in 1/3 of the required amount of demi water and heated to >80°C with a heated magnetic stirrer. The polymer gradually disperses to form uniform slurry. The remaining water was added as ice water after complete dissolution of the polymer to get rapid hydration. The solution was then cooled in an ice bath while vigorously stirring with an overhead stirrer at 500 rpm for 30 min. The clear aqueous solutions

TABLE II
Process Variables for fluidized Bed Coating experiments

Reactor	Fluid bed Dryer, two-way nozzle (spherical pattern)
Nozzle	Air-pressured (nozzle insert: 0.8 mm)[a]
Nozzle's position	Top-spray, ≈ 5 cm above the fluid bed. Constant position
Filter	Standard, not shaken
Coating solution spray rate, R_{sol}	1.2 g/min, peristaltic pump[b]: 3 rpm.
Mass of core material, W_p	150 g
Inlet air flow rate, F_i	60 Kg/h constant
Inlet air velocity	2.7 m/s
Fluid bed temperature	70°C, autom. kept constant by software
Inlet air temperature, T_1	75–80°C, autom. determined by software
Outlet air temperature, T_o	55–65°C, autom. recorded by thermometer
Atomizing air pressure	0.5 bar
Heating system temperature	100°C
Fluid bed relative humidity	Recorded by means of the software
Outlet air relative humidity	±3%, recorded by means of the software
Coating solution dry matter content, DM	3% w/w
particles coating content, w	9% w/w
Mass of coating solution, W_{cs}	494.5 g
Coating solution temperature, T_s	Room temperature
Drying time (after spraying)	10 min
Drying temperature (after spraying)	70°C

[a] Watson Marlow 505U, VWR International, Amsterdam, The Netherlands.
[b] Mettler Toledo PG8001-S, Mettler Toledo, Switzerland.

obtained were then allowed to hydrate overnight at 5°C and allowed to defoam and equilibrate at room temperature for several hours before use.

PVA was dispersed into cold water with continuous stirring. The mixture was heated to 90–95°C in a water bath. After dissolution of the polymer the solution was cooled down to room temperature with continuous stirring. The dissolution speed increased with increasing temperature and decreasing molecule size. Foam formation was minimized by making use of an overhead stirrer at low speed. Before use, the PVA solutions were set to room temperature. It is important to note that the viscosity of PVA solutions can increase with storage time.

Particle coating

A conical prototype fluidized bed unit (DSM Food Specialties, Delft, The Netherlands) was used for all coating experiments. The coating experiments were performed in the top-spray mode and the position of the two-way pneumatic air pressure nozzle was kept constant. The nozzle position was chosen such that the spray cone did not excessively contact the reactor wall.

The sodium benzoate particles were sieved in batches of 150 g. These batches were transferred to the fluidized bed reactor after the system was brought at steady state for 10 min. The coating solution was transported to the spraying nozzle using a peristaltic pump (Pump drive Watson Marlow 505U, VWR International, PA). The coating solution was kept at ambient temperature. The particles were fluidized at an inlet air velocity of 2.7 m/s. The spraying pressure (0.5 bar), inlet air flow rate (60 kg/h), coating solution flow rate (1.2 g/min), and the fluid bed temperature (70°C) were kept constant in all experiments. The coated particles were dried for 10 min at 70°C directly after fluidized bed coating. The coating dosage on the particle surface was analyzed by weighing the particles before and directly after the coating process. Half of each batch was stored at 23°C and 55% RH. The other half was stored at −18°C (25% RH). Table II gives an overview of the process variables.

Scanning electron microscopy

All the images were produced with secondary electrons using a Philips XL 20 SEM (electron source from conventional tungsten's filament) operated at acceleration voltage of 15 kV. Samples were prepared by attaching ∼ 15 particles to a metallic support with araldite adhesive and a thin layer of gold was applied using an Edwards Sputter Coater (pulse mode, 6 min plasma coating) to improve the conductivity and reduce charging.

Atomic force microcopy

The surface structure of the particle coatings was imaged with an AFM with a lateral resolution in the nanometer range. Polymer-coated particles were glued onto a glass slide using superglue. The sample

was mounted on the sample table of the AFM (XE 100 Park Systems, Iui-Dong, Korea) after hardening of the glue. The sample surface was scanned in contact mode with a contact force of 1 nN that was held constant by a feedback loop. A rectangular cantilever (37th series, Cantilever B, μmasch, Tallinn, Estonia) was used with a nominal force constant of 0.3 N/m and a probe tip radius of 10 nm. The images were recorded under ambient conditions.

Thermogravimetric analysis

Thermogravimetric analyses (TGAs) using a TGA 7 (Perkin Elmer, MA) with a dry nitrogen purge were performed to determine the water content of HPMC 603, HPMC 615, and PVA 4–98 coated Purox. Alumel (152.17°C) and Perkalloy (594.47°C) were used to calibrate the temperature reading and the weight measurement was calibrated using reference materials according to the manufacturer's instructions. Approximately 5–20 mg of HPMC 603, HPMC 615, and PVA 4–98 coated Purox were placed in alumina crucibles for TGA and the weight loss was measured during heating from 25°C to 150°C at a heating rate of 10°C/min followed by a constant temperature of 150°C for 10 min. The difference between the initial and the final sample weight was used as a measure for the water content of the samples. All measurements were repeated at least twice.

Repeated impact test

Repeated impact tests were used to determine the resistance of the particles to attrition in terms of remaining undamaged mass as function of the impact mass specific energy, $E_{i,m}$, in J/Kg [eq. (4)]. The impact mass specific energy considered corresponds to certain number of collisions in RIT and reflects attrition performance at a low, intermediate, and high number of collisions. Repeated impact tests were performed using approximately $\sim$ 200–300 mg particles each test. Each experiment was repeated at least three times and the results were averaged. The relative humidity and the temperature during experiments were kept constant at 50–65% and 23°C. Before performing RIT water content of each sample was measured by TGA (section 2.5).

In this study, the oscillation frequency and the amplitude were kept constant ($f = 40$ Hz, $A = 2.8$ cm). The resulting particle impact velocity (v_p) was 7.04 m s^{-1}. The particles were sieved using a mesh of 400 μm after each RIT experiment to remove debris created by the impacts from the original particles. The mesh size was chosen to retain undamaged particles and to allow the passage of fractured particles. The particles were carefully weighed (Mettler Toledo balance AX205DR, Switzerland) before and after the RIT to determine the remaining mass (m_{rm}) using eq. (3). All the RIT tests are repeated in triple.

The coefficient of restitution was determined by free-fall impact tests, where particles were dropped from a height of 120 cm and impacted with a steel plate of the same material as the box used in the RIT experiments. The impact was recorded with a high speed camera at 1000 fps (Phantom v5.0). The coefficient of restitution was determined by calculating the ratio between the velocities before and after impact. Each measurement was repeated at least eight times and the average value was used. Because of their irregular shape, the bouncing of the particles was not always perfectly vertical. In addition, the elastic strain energy was in some cases transformed into rotation energy, which could not be determined from the experiment. Rotating particles and particles with a nonvertical trajectory were neglected in the calculations.

Nanoindentation

Sample preparation

Coated polymer particles were embedded in a two-component-epoxy-adhesive keeping the top sticking out of the glue. The bottom side of the particle was in contact with the sample holder. Before performing quasistatic and dynamic nanoindentation, the water content of each sample was measured by TGA (section 2.5).

Indentation procedure

Quasistatic and dynamic indentation experiments were carried out with a commercial nanomechanical testing system (TriboIndenter®, Hysitron, Minneapolis, MN). The system had normal load and displacement noise floors of 0.1 μN and 0.2 nm, respectively. A three-sided pyramidal diamond indenter tip, so-called Berkovich tip, was used for the experiments. Before testing, the machine compliance and the tip-area-function were determined by standard procedures[21] using fused silica as calibration standard. Defined positions on top of each particle were chosen using the optical microscope integrated into the nanoindenter device. Subsequently, the particle was moved under the Berkovich tip with a positioning accuracy of 0.5 microns. All indentation tests were performed under ambient conditions (relative humidity: 50–65%, temperature: 23°C). Particles that were stored at –18°C were thawed and then measured within one day.

Quasistatic nanoindentation testing was carried out in a load controlled manner. The tip was contacted with the specimen surface at a preset contact force of 1 μN. Following the initial contact procedure, the tip was lifted 10 nm, and then, driven into

the surface with a loading rate of 100 μN/s until a peak load of 1000 μN was reached. The tip was kept at constant position for 2 s, when the peak load was reached. Unloading was performed at a rate of 100 μN/s. During this trapezoidal loading-unloading cycle, the displacement of the indenter was recorded and a corresponding load-displacement dataset was obtained.

Before testing, the stiffness, the damping, and the mass of the sensor were determined by running a frequency sweep in air. The values for the stiffness and the damping of the sensor were then subtracted from the measured values to obtain the net sample response.

In this work, the indenter was quasistatically driven into the sample until a start load of 1000 μN was reached. The peak or end load of 4000 μN was approached in 15 discrete depth steps. At each depth step, the oscillatory force was applied with a force amplitude of 15 μN and a frequency of 75 Hz. The magnitude of the force amplitude was adjusted so that the resulting displacement amplitude was roughly 1–2 nm. Higher amplitudes should be avoided because of potential plastic deformation behavior. Moreover, preliminary tests had shown that the frequency had no influence on the dynamic mechanical parameters of all samples between tested frequencies of 10–200 Hz. For each particle 10 indents at positions 15 μm apart of each other were performed.

The bending of the particle surface was neglected for data analysis—a flat surface was assumed. This assumption is reasonable as the dimensions of the particle (>1 mm) drastically exceed the lateral dimensions of the indentation (a few microns).

When working with coating layers a possible influence of the underlying substrate on the indentation results—the so-called substrate effect—has to be taken into account. According to a rough rule of thumb, the indentation depth should not exceed 10% of the coating thickness. Even tough, this is a widely used procedure when probing thin films this rule has no physical basis.[19,36] Measuring mechanical parameters as a function of the indentation depth is another possibility to get an indication whether the coating alone is probed or whether the substrate has an influence.

RESULTS AND DISCUSSION

Morphological characterization

Two types of hydroxypropyl methylcellulose (HPMC 603 and HPMC 615) and PVA 4–98 were studied. Coated particles were first analyzed using SEM to assess their coating thickness and the coating surface morphology. The thickness of the coating layer was estimated on the basis of SEM pictures by analyzing at least three particles. For each particle, the thickness was measured at least at five different positions. Average values are reported. Quantities of coating solutions with the corresponding dry basis coating fraction and the SEM-measured ones are listed and compared in Table III.

TABLE III
Details on Particle Coatings

Coating polymer	Coating solution (g)	Theoretical coating fraction (% w/w db)	Thickness[a] (μm)
HPMC 603	494.5	9	20.53 ± 3
HPMC 615	494.5	9	21.01 ± 2.5
PVA 4–98	494.5	9	20.16 ± 2.9

[a] SEM.

Figure 2 gathers SEM micrographs of Purox coated with PVA 4–98, HPMC 603, and HPMC 615. Per each coating material a macrolevel, a microlevel, and a cross section picture are presented.

Figure 2 also shows a morphological comparison between the three different coatings in terms of storage temperature, room temperature (left part of the figure), and at −18°C (right part of the figure). SEM micrographs of coated Purox particles with the three different coating agents revealed similarities in coating quality. The core particles are uniformly covered in all three cases. The coating films are all formed by coalescence of droplets sprayed on the surface of the core particle. The coalescence of these droplets is pretty good and homogenous for all the three materials. In some cases, the droplets become dry before complete coalescence is accomplished. This leads to the formation of bumps and craters in the coating.

The surfaces of the PVA 4–98 were rougher than the HPMC 603 and HPMC 615 coatings that were dosed at similar concentrations. All three coatings had small cracks on their surfaces. These cracks were likely to be caused by particle–particle and particle–wall collisions during coating process. The cracks were more evident when thicker coating layers were applied, which could be (partly) related to the residence time of the particles in the fluidized bed. No major differences could be observed between samples that were stored at room temperature or at −18°C. HPMC 615 coating showed smaller deviations of coating thickness than those from PVA 4–98 and HPMC 603. Thicker coating layers were observed in proximity of "valleys" of core particle.

The AFM images, in Figure 3, depict the structural details of the surfaces of the PVA 4–98, HPMC 603, and HPMC 615 coatings. Per each type of coating material samples stored at room temperature (line on the top of Fig. 3) and at −18°C (bottom line of Fig. 3) are presented.

The droplet size seems to vary randomly. This is because of the variation in droplet and particle

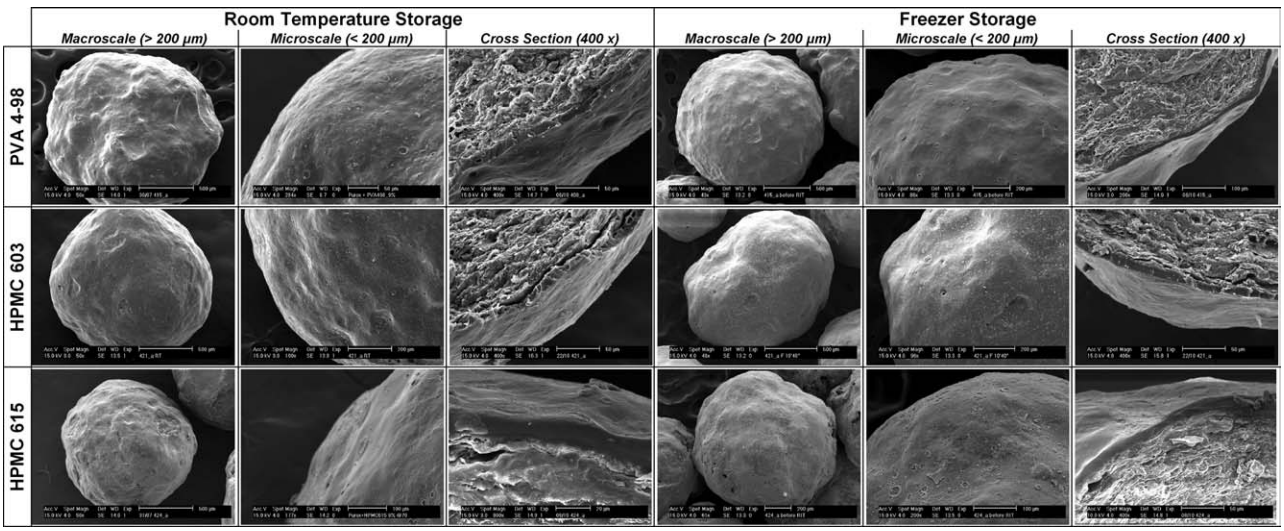

Figure 2 Scanning electron microscope micrographs of Purox-S coated with the three different coating agents PVA 4–98, HPMC 603, and HPMC 615 from the top to the bottom.

trajectory in the fluidized bed. For example, droplets will be smaller when it travels a longer distance before hitting a particle as the result of water evaporation. All process parameters were kept constant (i.e., spraying pressure, fluid bed temperature, and spraying rate), which implies that the droplet size is mainly related to the viscosity of the coating solution and the droplet trajectory. Besides droplets, there are also other structures visible on the coating surface. These structures are probably caused by the attachment of dust to the coating surface.

Thermo gravimetric analysis

Before performing repeated impact tests, quasistatic, and dynamic indentation the water content of each

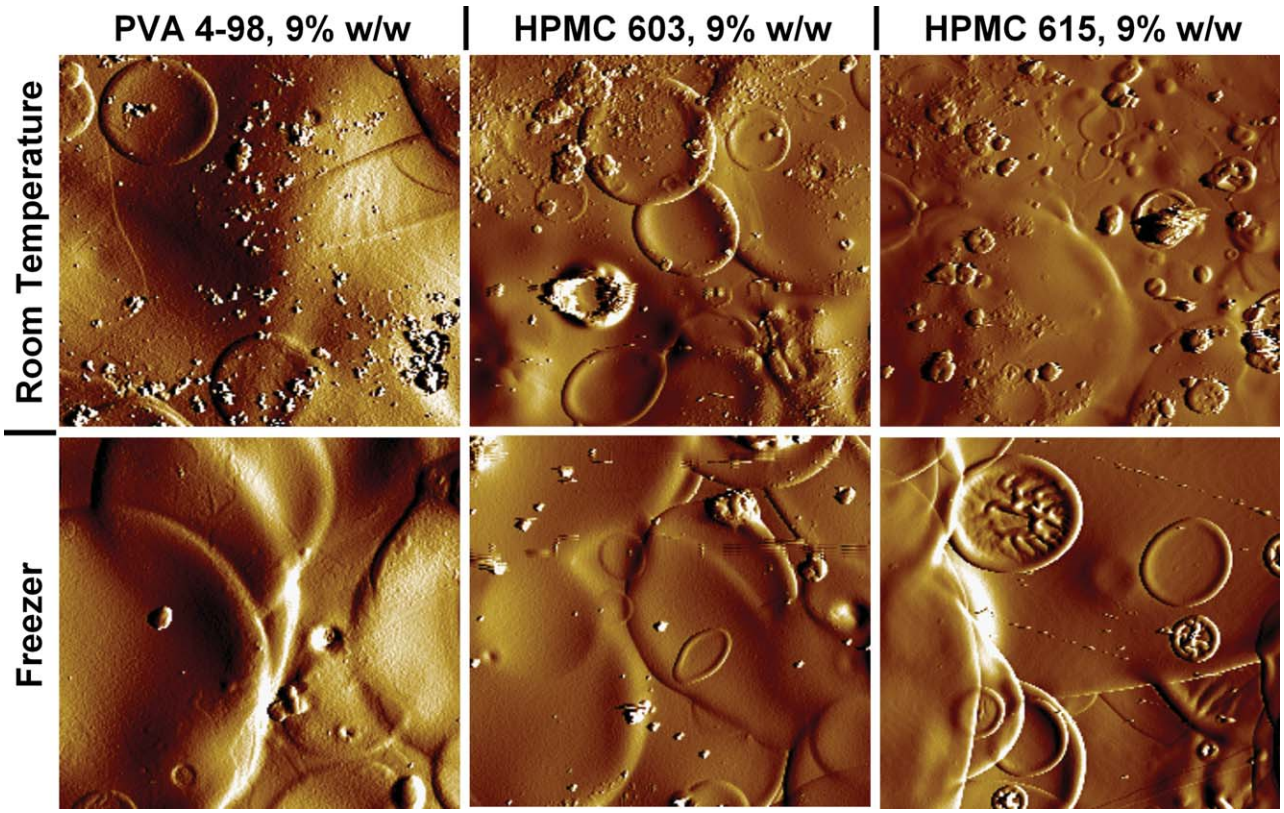

Figure 3 AFM images of coating surfaces at a scan size of 40 µm x 40 µm. [Color figure can be viewed in the online issue, which is available at www.interscience.wiley.com.]

TABLE IV
Water content, Average Value and Standard Deviation, of the Samples (by TGA) before Performing RIT, Quasistatic and Dynamic nanoindentation

	W_c [%]			
	Room temp.		Freezer	
	Avarage	STD	Avarage	STD
PVA 4–98	0.85	0.156	1.09	0.0354
HPMC 603	0.55	0.099	0.77	0.0283
HPMC 615	0.53	0.085	0.69	0.0354

sample was measured by TGA (section 2.5). In Table IV, the water content (average value and its corresponding standard deviation) for all the samples are listed.

For PVA 4–98, HPMC 603, and HPMC 615, the particles stored at –18°C present higher water content regardless the lower relative humidity in the freezer compared with ambient conditions. This was explained by condensation of moisture onto the external surface of the coated particles after removing them from the freezer. For PVA 4–98, such difference is in the order of 0.24%, while is 0.22% for HPMC 603 and 0.16% HPMC 615.

Mechanical characterization using repeated impact testing

RIT was used to measure resistance to attrition of coated particles. Table V depicts the relation between time of impacting, the number of impacts, the mass specific kinetic energy ($E_{k,m}$), and mass specific energy of impact ($E_{i,m}$) generated by the RIT apparatus with present setup for a reference 1 mg sample of Purox coated with HPMC 615 stored at room temperature (reference coefficient of restitution, $e = 0.59$).

Resistance to attriti on of particles coated with different polymer agents are compared, which means, given Purox-S as common core particle and for the determined water contents, a comparison between the three chosen polymer coatings. Additionally, differences in resistance to attrition between coated

TABLE V
Example of Typical Data Gathered from Repeated Impact Testing Using the Preset Setup Described in Section 1.1 (Coefficient of Restitution, $e = 0.59$)

Time (min)	Impacts (N)	$E_{k,m}$ (J/kg)	$E_{i,m}$ (J/kg)
0	0	0	0
5′20″	25600	634	259.94
10′40″	51200	1269	520.29
21′20″	102400	2537	1040.17
42′40″	204801	5074	2080.34
85′20″	409600	10138	4156.58
128	614400	15120	6199.2
170′40″	819200	20018	8207.38

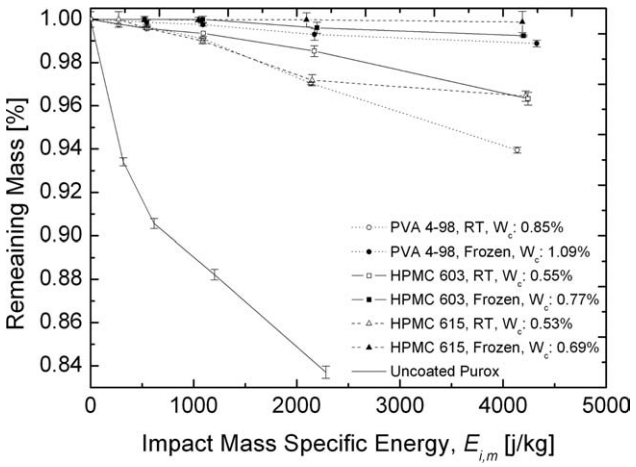

Figure 4 RIT results for Purox-S uncoated (-) and Purox-S coated with 9% w/w PVA 4–98 (○, ●), HPMC-603 (□, ■), and HPMC 615 (▲, Δ). ($A = 3.8$ cm, $f = 40$ Hz, and $v_p = 7.04$ m s^{-1}).

particles stored at −18°C (25% RH) and those stored at ambient conditions (23°C and 55% RH) were highlighted. The coefficients of restitution were estimated to be 0.57, 0.57, and 0.59 for Purox-S coated with PVA 4–98, HPMC 603, and HPMC 615, respectively.

Figure 4 shows the remaining mass of Purox-S coated with 9% w/w coating PVA 4–98, HPMC 603, and HPMC 615 as function of the mass specific energy of impact, $E_{i,m}$, for particles that were stored at ambient conditions (empty symbols) and at −18°C (full symbols). The standard deviation per each data point is presented as error bars. As reference, uncoated Purox-S is tested and the results are also shown in Figure 4 as well as the water content (average value) of each sample before RIT (legend of Fig. 4).

Overall, the HPMC 615 coating performs the best during both long and short periods of attrition. At short periods, corresponding to low values of impact mass specific energies applied in RIT, HPMC 603, and PVA 4–98 coating perform equally, but they fail at longer periods of attrition. Uncoated Purox-S shows very scarce resistance to attrition. At low impact mass specific energies uncoated Purox-S has high attrition rate. The initial high attrition rate corresponds to the peeling mechanism.[16] At higher number of collisions, the attrition rate follows a linear decay, corresponding to the erosion mechanism.[16] The initially high attrition rate is because of the removal of surface asperities of the Purox-S. When a coating layer is applied on the Purox-S particles, a lower attrition rate is observed as consequence, which results, of course, in a stronger particle toward attrition. HPMC 615 stored at −18°C does not show any attrition, not showing any loss of mass (Fig. 4). This means the coating is strong

enough to survive RIT conditions. On the contrary, HPMC 615 coating on Purox-S stored at RT initially shows no attrition until ~ 1500–2000 J/kg, when the coating starts to fail (Fig. 4). This type of failure is a typical layer fatigue mechanism.[16] The coating starts to crack at a certain threshold and once the cracks grow, the coating fails quickly. Purox-S coated with HPMC 603 stored at RT (Fig. 4) does show a small attrition until 1000 J/kg. Only after ~ 1000 J/kg, the coating starts to fail. Purox-S coated with HPMC 603 and stored at RT, Purox-S coated with PVA 4–98, and stored at −18°C, Purox-S coated with PVA 4–98 and stored at RT show immediately loss in mass because of the removal of surface irregularities (Figs. 2 and 3). Still the attrition rate results to be quite low. Increasing the impact mass specific energy, the attrition rate tends to increase leading to 3.5, 3.5, and 6% loss in weight.

In general, particles stored at −18°C show higher resistance to attrition, no matter the coating agent chosen. For all three coating types, the difference is negligible at low impact energy (below 1.5 KJ/kg). At higher impact energies a difference in the range of 2.5–3% becomes visible especially in the case of PVA 4–98 and HPMC 603. The reasons of this trend might be because of the combined effect of the different water content of the particles and the polymer morphology in relation to their storage conditions. In fact, in all three cases, the coated particles stored in the freezer contain higher water content. The plasticizing effect of the water in a polymer matrix is well known. Such water, placed all around the surface of the particles and within the structure, makes the polymer chains to flip over each other, and thus, to be more ductile and viscoelastic and more resistance to fatigue. The structure of the coating shell, thanks the flexibility effect of the water, adsorbs and reacts bouncing much more elastically, avoiding cracks and damages. Therefore, these particles combine the ideal elastic properties, which make the particles resisting to stresses bouncing elastically, and the viscous properties, which enable the particles to absorb and release stresses without cracking, given by the plasticizing effect of the water in the structure.

The breakage mechanism of all coated particles seems to be layer fatigue.[16] The peeling mechanism is, in fact, insignificant and the particles have good resistance against attrition at low energy until a critical impact energy is reached above, which the resistance against attrition is significantly reduced.

The attrition observed during RIT of coated Purox-S would be, in theory, a combination of attrition of the coating shell and the Purox-S. As even at longest periods of RIT, the losses in weight are always lower than 9% w/w of coating applied the attritions observed on coated Purox-S that are accounted to the coating material only.

The attrition of the particle and the evolution of the breakage mechanism was also observed by SEM. Figure 5 gives an overview of SEM pictures of Purox-S particles coated with 9% of PVA 4–98, HPMC 603, and HPMC 615 before RIT, after 10′40″ in RIT ($E_{i,m} \approx 520.29$ J/kg), after 42′40″ in RIT ($E_{i,m} \approx 2080.34$ J/kg), and after 85′20″ in RIT ($E_{i,m} \approx 4156.58$ kJ/kg). It appears that the particles are successively experiencing the three types of attrition mechanisms proposed by Beekman et al.[16]: (1) peeling, (2) erosion, and (3) layer fatigue confirming the trends of the data obtained by using RIT.

After the first 11 min under repeated impacts, the coated particles are still intact even though some fractions have been removed as the result of attrition. After 43 min of RIT, the sharp edges and asperities (Figs. 2 and 3) are removed from the surface of the coated particles and few cracks become visible in the coating layer. This indicates that the main breakage mechanism is peeling. Subsequently, the coating is removed mainly around the cracks as the result of erosion. After 85 min of RIT, large pieces of the coating layer are removed because of the layer fatigue resulting in a fast increase of the attrition rate.

Mechanical characterization using nanoindentation

The samples that were studied using RIT were also investigated by quasistatic and dynamic nanoindentation to measure the viscoelastic properties, such as E', E'', and Tan δ, of the polymeric coating layers.[37] The resistance to attrition measured with RIT, in fact, was only accounted to the coating materials and not to core particles. This would enable us to figure out, which of these characteristics are responsible of making the coating stronger, and thus, more resistant-to-attrition coated particles. Before quasistatic and dynamic nanoindentation, the water content of the samples was measured by TGA (Table IV).

Quasistatic measurements

Figure 6 depicts force-displacement curves for PVA 4–98 [Fig. 6(a)], HPMC 603 [Fig. 6(b)], and HPMC 615 [Fig. 6(c)] coatings as a function of the storage conditions. Water contents of all the samples are listed in Table IV. A quantitative analysis of the data sets of the quasistatic indents is very difficult because the standard analyzing techniques (e.g., the Oliver–Pharr Method[20]) do not account for time-dependent behavior, which is typical for polymeric materials. Nonetheless, the obtained data sets provide valuable information on the deformation characteristics and allow for comparison of particles

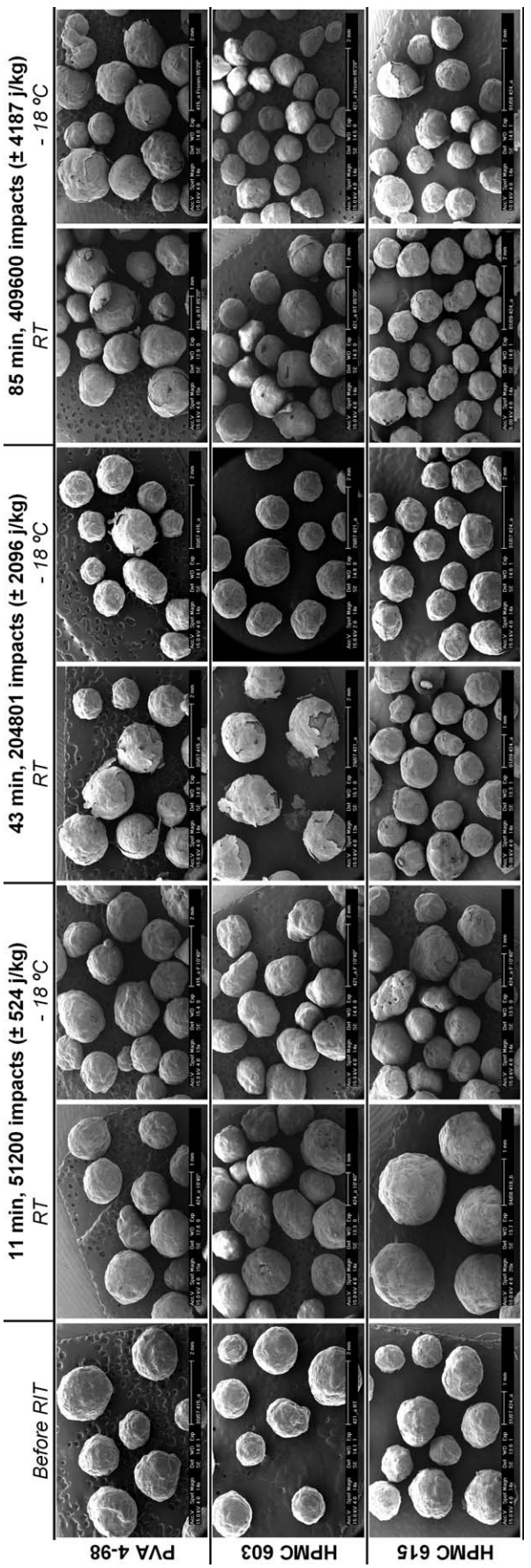

Figure 5 SEM micrographs (magnification: 14x) of Purox-S coated with PVA 4–98, HPMC 603, and HPMC 615 at different RIT times ($f = 40$ Hz, $A = 3.8$ cm, and $v_p = 7.04$ m s^{-1}).

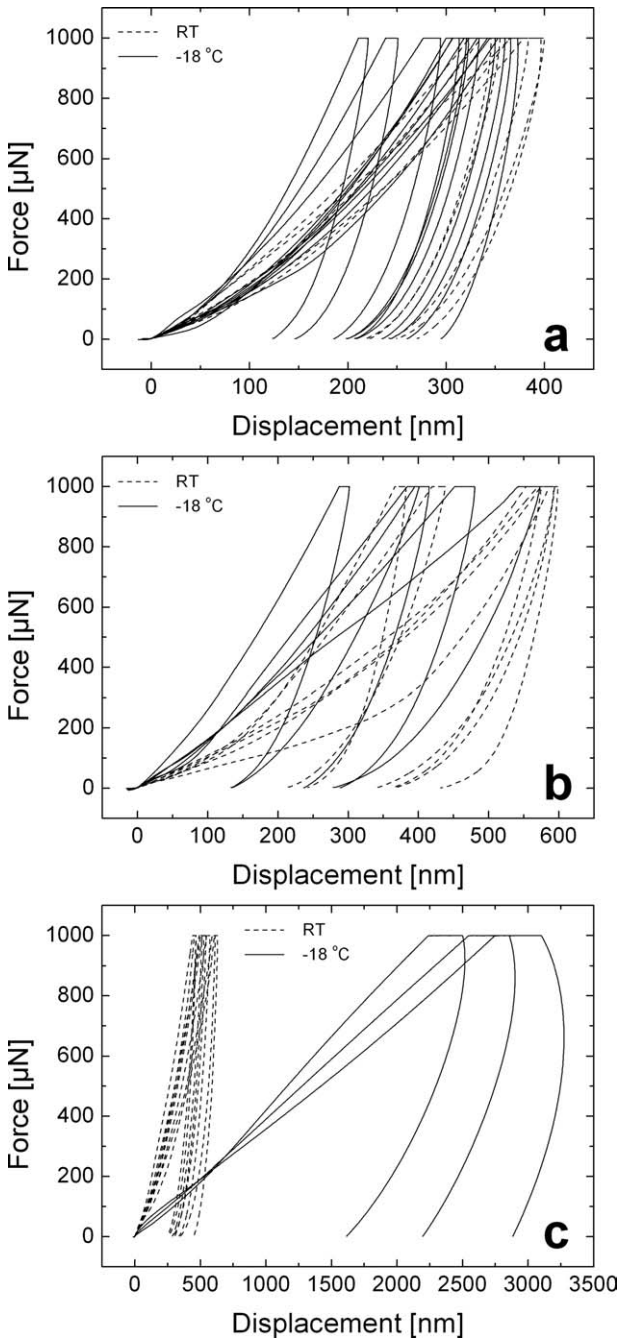

Figure 6 Force-displacement datasets of quasistatic indentations for Purox coated with 9% w/w PVA 4–98 (a), HPMC 603 (b), and HPMC 615 (c) for room temperature (dashed line) and −18°C (solid line).

coated with different coating agents in terms of the two storage conditions taken in exam.

All datasets show a strong hysteresis between the loading and the unloading branch. In addition, a distinct residual deformation after unloading is visible in all cases. For purely elastic behavior hysteresis or residual deformation would not be observed. Hysteresis and residual deformation are caused by viscous and/or plastic behavior. At the peak force of 1000 µN, the force is kept constant for 2 sec. During this time, the material creep, which is characteristic for polymeric materials, is detectable. The unloading curves of this polymer coating are clearly "belly-shaped," i.e., at the beginning of unloading the indentation depth is still increasing although the load is decreased. This deformation behavior during unloading is also caused by material creep.

When comparing the different coating agents stored at room temperature, Figure 6 shows that PVA 4–98 yields, at maximum load, the least being the maximum displacement in range of 315–385 nm. In that sense, PVA 4–98 presents the highest resistance against quasistatic deformation followed by HPMC 603 with a maximum displacement of 375–550 nm, and HPMC 615 with a maximum displacement of 550–675 nm. For particles stored at −18°C similar displacements can be noticed in case of PVA 4–98 and HPMC 603, whereas HPMC 615 sample that was stored at –18°C shows a more pronounced creep (2000–3000 nm) than the other coatings [Fig. 6(c)].

The storage conditions (RT or –18°C) do not influence the deformation behavior of the PVA 4–98 and HPMC 603 coatings [Fig. 6(a,b)]. For these polymer coatings, the shape of the curves and the maximum displacement at peak load is independent of storage conditions. In this type of not-dynamic stress, in fact, the plasticizing effect of water results not to be relevant. This is different in the case of HPMC 615 coatings. Here, the sample shows more creep and a higher maximum displacement at –18°C in comparison to the sample stored at RT. This indicates that the water content plays an important role for the deformation confirming the results obtained with RIT. The fact that HPMC 603 and PVA 4–98 show storage-independent behavior might denote that entrapped water during the freezing process is released very soon at ambient conditions. HPMC 615 has a higher molecular weight than the HPMC 603. It is likely that because of the longer polymer chains, the molecular structure of HPMC 615 is more entangled. This branched polymer network could entrap water more easily, which is not released at ambient conditions (Table IV).

Dynamic measurements

The dynamic mechanical parameters E', E'', and tan δ were determined at 15 discrete load steps and 15 contact depths. Figure 7 shows the measured values for E' and E'' as a function of the contact depth for one indentation carried out on a HPMC 603 coated particle. The graph shows that there is no depth dependence observable, neither for the storage modulus nor for the loss modulus. For all samples, no

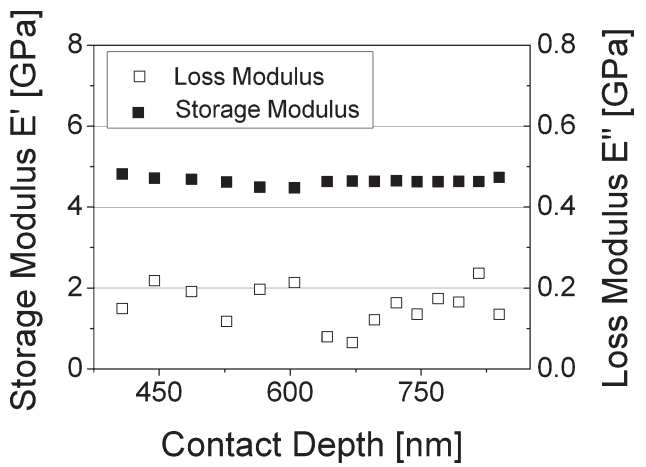

Figure 7 Dynamic indentation measurement performed on a HPMC 603-coated particles stored at room temperature.

depth-dependent trends of the dynamic mechanical parameters could be observed within the investigated load range (1000–4000 μN). This strongly supports the assumption that a potential substrate effect is not present (compare 0).

Ten indentations, 15 μm apart each other, were performed on each particle. The results of 10 particles were averaged. Figure 8 depicts the storage modulus (E') [Fig. 8(a)], the loss modulus (E'') [Fig. 8(b)], and the damping factor (tan δ) [Fig. 8(c)] for PVA 4–98, HPMC 603, and HPMC 615.

The storage modulus E' [Fig. 8(a)], which reflects the elastic portion of the material behavior and is a measure for the energy stored in a reversible way, corresponds with the maximum displacement obtained from the quasistatic nanoindentation tests. The maximum displacement decreases with increasing E'. In this respect, PVA 4–98 present the highest E', 11 GPa, followed by HPMC 603, 5.5–6 GPa, which is higher than HPMC 615, 1.5–2 GPa in agreement with data present in literature for corresponding cast film.[37,35] The internal damping expressed by E'' [Fig. 8(b)], which denotes the viscous part, and is thus a measure for the energy dissipated into heat per period of stress, is much higher for PVA in comparison with the two HPMC coatings, in the order of 0.6 GPa for PVA 4–98, and 0.2 GPa for both HPMC 603 and HPMC 615.[37,35] There is no difference between storage at RT and –18°C for PVA 4–98 and HPMC 603, which is in agreement with the quasistatic measurements. On the contrary, E' and E'' of the HPMC 615 coating that was stored at –18°C is smaller compared with the particle stored at RT reflecting the differences assessed by quasistatic tests.

Tan δ reflects the ratio of viscous and elastic material behavior. The highest tan δ values are obtained for the HPMC 615 sample [Fig. 8(c)] followed by PVA 4–98 and HPMC 603 having a Tan δ of 0.15, 0.05, and 0.04, respectively. For HPMC 615, a much more viscous behavior is observed for the coating that was stored at −18°C, which might be a result of entrapped water that is not immediately released upon thawing. The dynamic nanoindentation measurements confirm that in case of PVA 4–98 and HPMC 603, the coating mechanical behavior is independent of the storage conditions as established with quasistatic tests. Comparing only the RT samples with each other reveals that HPMC 615 behaves in a more viscous manner than PVA 4–98 and HPMC 603, whereas the

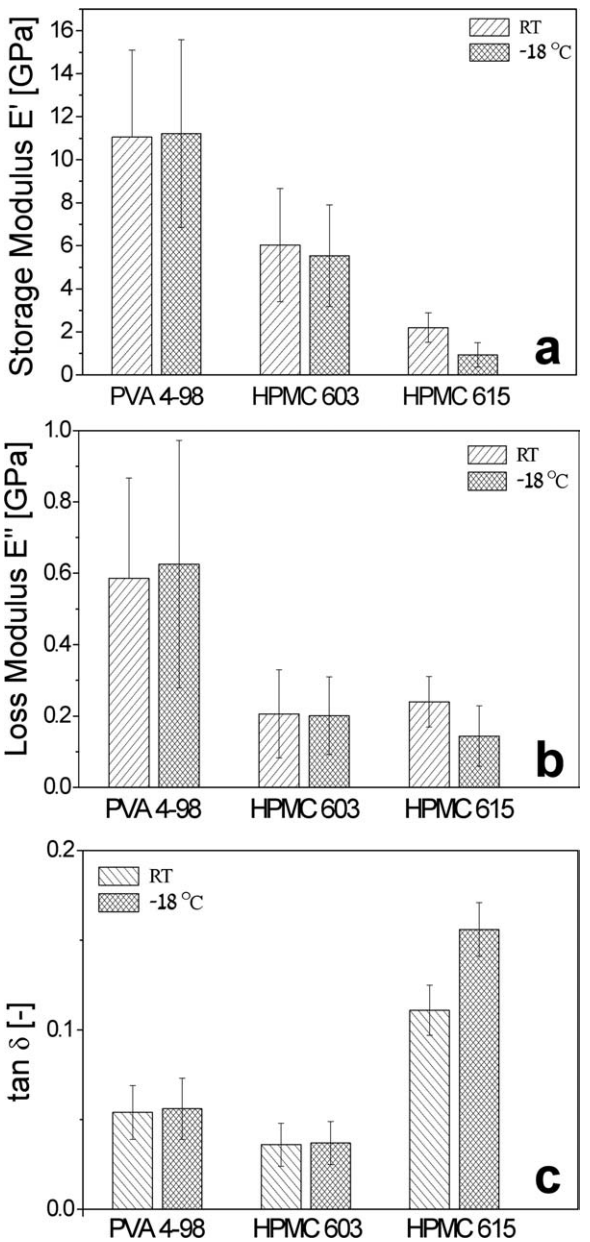

Figure 8 Averaged dynamic mechanical parameters (E', E'', and tan δ) for PVA 4–98, HPMC 603, and HPMC 615. Ten particles were averaged for each data point. On each particle 10 indentations were performed. The error bars correspond to the pooled standard deviation.

differences between the two latter ones are neglectable considering the standard deviations.

The error bars (standard deviation) are much larger for E' and E'' compared with tan δ. This is caused by the fact that tan δ does not depend on the projected contact area A_c. The SEM and the AFM images have shown distinct asperities on all sample surfaces (compare 0). This surface roughness may lead to uncertainties in the determination of A_c and indirect to a scatter of the E' and E'' data. In the present case, tan δ is a more robust parameter that is unaffected by the surface roughness (compare 0).

Comparison of RIT and nanoindentation

Performing repeated impact testing on Purox-S coated with different coating agents enabled us to measure the resistance to attrition of such coated particles and in the end figure out which coating material behaves better and make the coated Purox-S more resistant to attrition. By means of nanoindentation tests, we could assess the viscoelastic properties of the coating layers theirself, which are responsible of their mechanical behavior resistance. It appears that HPMC 615, which has clearly the highest tan δ value, is also the most attrition-resistant sample (Fig. 4). HPMC 603 and PVA 4–98 have very similar tan δ values [Fig. 8(c)]. Both samples show only minor differences in their attrition resistance (Fig. 4). These observations indicate that tan δ correlates with the attrition resistance of the coated particles. The higher tan δ, i.e., the more viscous the material the more attrition resistant it behaves. The high viscoelastic nature of HPMC 615 coating permits the coated particles to adapt better to the repeated impacts stress. From one side, the elastic component of HPMC 615 allows the material to do not dissipate energy and to do not deform when the stress is repetitively applied. Moreover, it makes the particles more rigid and inflexible. On the other side, the viscous part of HPMC 615 increases the absorption of energy when such stress is applied resulting in creep and stress relaxation. Such stress relaxation makes the material to relax and to flexibly accommodate the imposed stresses and strains generated by repeated impacts. The shape change, following creeps and viscoelastic behavior, is responsible of the preservation of coated particles integrity. Whereas, an elastic and brittle material as PVA 4–98 has the memory only of its reference shape, the instantaneous deformation of a highly viscoelastic material as HPMC 615 is a function of the entire history of applied force. Conversely, the instantaneous restoring force is a function of the entire history of deformation, repeated impact, or indentations. In this case, the internal forces depend not only on the magnitude of deformation but also on the rate of deformation. Therefore, rigid and inflexible materials would be quite inappropriate for protecting the coated particles under repeated impacts. It has been confirmed, in fact, that even if PVA 4–98 and HPMC 603 showed the highest E' and E'', their tan δ as measure of their viscoelasticity and flexibility were lower than the one measured for HPMC 615.

The relatively small differences in E', E'', and tan δ of PVA 4–98, when the samples stored at RT versus those at −18°C (Fig. 8), are accompanied with relatively large differences in remaining mass, m_{rm} (Fig. 4). This can be explained considering the different nature of the two measuring systems, the influence of surface roughness on the nanoindents and the relatively high standard deviation in the indentation data. Moreover, the coating-core-interface behavior plays a crucial role for the attrition behavior, whereas it does not affect nanoindentation testing. Nevertheless, good correlation could be noticed between quasistatic and dynamic indentation test (Fig. 6 vs. Fig. 8) and between these and the resistance to attrition measured with RIT (Fig. 6, Fig. 8 vs. Fig. 4). Overall the results are indicative of the fact that a combined nanoindentation–RIT approach is needed, when one wants to clarify and explain the overall behavior against attrition of polymeric coated particles.

CONCLUSIONS

Polymer-coated particles were successfully obtained and mechanically characterized by applying repeated impacts and nanoindentation tests. The results are indicative of the fact that the polymer coating intrinsic properties can be successfully related to the resistance to attrition.

The resistance to attrition behavior of the chosen reference coated particles was measured as remaining mass function of impact mass specific energy $Ei_{,m}$. The resistance to attrition was discussed in terms of different coating agent, breakage mechanisms, and storage temperature (RT vs. −18°C). HPMC 615 resulted to offer the best protection against repeated impacts followed by HPMC 603 and PVA 4–98. The differences in performance are not relevant at low impact energy, corresponding to low number of collisions in RIT, whereas tend to drastically increase once this energy gets higher. Evident was the effect of storage temperature. At low impact energy in RIT the impact of storage conditions was negligible but at high impact energy (>1000 J/kg) the influence of storage conditions was clear. In all the three coating materials, the particles stored at −18°C were found to present higher water content (Table IV) than the ones stored at room temperature. Particles stored at −18°C had a higher resistance to attrition in RIT. Such difference could be stated in the range of 2.5–3% for HPMC 603 and

PVA 4–98, while ~ 3.5% for HPMC 615 (Fig. 4). Such improvement in the resistance is probably because of the combination of plasticizing effect of water content, which is responsible of improved ductility and viscoelasticity of the more resistant particles. The main results of quasistatic and dynamic nanoindentation are in agreement with each other. PVA 4–98 has the highest elastic stiffness of all investigated samples, followed by HPMC 603 and HPMC 615, which shows the lowest elastic stiffness. Tan δ is significantly higher for HPMC 615 compared with the two other samples, i.e., HPMC 615 behaves more viscous than the other two samples. The comparison of the nanoindentation results and those from RIT shows that tan δ is related to the attrition behavior. The results obtained in this work indicate the viscoelasticity, measured by nanoindentation, to be one of the causes of higher resistance to attrition. High viscoelasticity (high tan δ) makes the coating shells more ductile and flexible, and thus, more adapt to survive continuous-repeated impact stresses.

HPMC 615 coatings showed storage-dependent behavior, while HPMC 603 and PVA 4–98 coatings did not (Figs. 6 and 8), whereas strong storage influence was observed when testing with RIT. The different nature of the two measuring systems, the influence of surface roughness on the nanoindents, the relatively high standard deviation in the indentation data and the coating–core interaction in RIT are assumed to be responsible of that. Nevertheless, this work demonstrates that the complex mechanical behavior of coated particles cannot be characterized with a single analysis method. A combination of different methods is required to get a complete understanding of the relation between coating properties and the resistance to attrition. It is only by careful design in matching product daily-life application and coating material that one can really develop a coated particle, which is perfectly corresponding to the product function. Moreover, it has been demonstrated that in an engineering approach, an extended and appropriate characterization of the basic, intrinsic properties of the raw coating material is essential to fully understand their final performance.

References

1. Depypere, F.; Dewettinck, K.; Ronsse, F. Appl Biotechnol Food Sci Pol 2003, 1, 75.
2. Dezarn, T. J. In Encapsulation and Controlled Release of Food Ingredients; Risch, S. J., Reineccius, G. A., Eds.; American Chemical Society: Washington DC, 1995; pp 74–86.
3. Reineccius, G. A. In Encapsulation and Controlled Release of Food Ingredients; Risch, S. J., Reineccius, G. A., Eds.; American Chemical Society: Washington DC, 1995; pp 8–25.
4. Wan, L. S. C.; Heng, P. W. S.; Chia, C. G. H. Drug Dev Ind Pharm 1992, 18, 997.
5. Chulia, D. In Handbook of Powder Technology; Chulia, D., Deleuil, M., Pourcelot, Y., Eds. Elsevier: Amsterdam, 1994; pp 115–163.
6. Kester, J. J.; Fennema, O. R. Food Technol 1986, 40, 47.
7. Balassa, L. L.; Fanger, G. O. Food Technol 1971, 2, 245.
8. Duxbury, D. D.; Swientek, R. J. Food Proces 1992, 53, 38.
9. Kanawjia, S. K.; Pathania, V.; Singh, S. Indian Dairyman 1992, 44, 280.
10. Hegenbart, S. Food Prod Des 1993, 3, 28.
11. Ashady, R. J Microencapsul 1993, 10, 413.
12. Jackson, L. S.; Lee, K. Lebensm-Wiss Technol 1991, 24, 289.
13. Janovsky, C. Cereal Food World 1993, 38, 85.
14. Dziezak, J. D. Food Technol 1988, 42, 136.
15. Verkoeijen, D.; Meesters, G. M. H.; Vercoulen, P. H. V.; Scarlett, B. Powder Technol 2002, 124, 195.
16. Beekman, W. J.; Meesters, G. M. H.; Scarlett, B.; Becker, T. Part Part Syst Charact 2002, 19, 5.
17. Pitchumani, R.; Arce Strien, S.; Meesters, G. M. H.; Schaafsma, S. H.; Scarlett, B. Powder Technol 2004, 140, 240.
18. Van Laarhoven, B.; Wiers, S. C. A.; Schaafsma, S. H.; Meesters, G. M. H. Chem Eng Sci 2008, 63, 361.
19. Fischer-Cripps, A. C. Nanoindentation; Springer Verlag: New York, 2004.
20. Oliver, W. C.; Pharr, G. M. J Mater Res 1992, 7, 1564.
21. Hay, J. L.; Pharr, G. M. Instrumented indentation testing, In: Kuhn, H., Midlin, D., Eds.; ASM Handbook Mechanical Testing and Evaluation; ASM International, Materials Park, OH, 2000, pp 232–243.
22. Oliver, W. C.; Pharr, G. M. J Mater Res 2004, 19, 3.
23. Vanlandingham, M. R. J Res Natl Inst Stan 2003, 108, 249.
24. Hayes, S. A.; Goruppy, A. A.; Jones, F. R. J Mater Res 2004, 19, 3298.
25. Herbert, E. G.; Oliver, W. C.; Pharr, G. M. J Phys D Appl Phys 2008, 41, 1.
26. Odegard, G. M.; Gates, T. S.; Herring, H. M. Exp Mech 2005, 45, 130.
27. Loubet, J.-L.; Lucas, B. N.; Oliver, W. C. Some measurements of viscoelastic properties with the help of nanoindentation Conf. Proc. Int. Workshop on Instrumented Indentation (San Diego, CA, 22–23 April 1995) ed D T Smith (Washington, DC: NIST) (Special Publication 896), 1995, pp 31–34.
28. Bouaita, N.; Bull, S. J.; Fernandez Palacio, J.; White, J. R. Polym Eng Sci 2006, 46, 1160.
29. Loubet, J. L.; Oliver, W. C.; Lucas, B. N. J Mater Res 2000, 15, 1195.
30. Park, K.; Mishra, S.; Lewis, G.; Losby, J.; Fan, Z.; Park, J. B. Biomaterials 2004, 25, 2427.
31. Sikdar, D.; Katti, D.; Katti, K.; Mohanty, B. J Appl Polym Sci 2007, 105, 790.
32. Chakravartula, A.; Komvopoulos, K. Appl Phys Lett 2006, 88, 131901.
33. Zhou, J.; Komvopoulos, K. Appl Phys Lett 2007, 90, 021910.
34. Lu, Y. C.; Shinozaki, D. M. Exp Mech 2010, 50, 71.
35. Perfetti, G.; Jansen, K. M. B.; Wildeboer, W. J.; Van Hee, P.; Meesters, G. M. H. Int J Pharm 2010, 384, 109.
36. Bull, S. J. J Phys D Appl Phys 2005, 38, 393.
37. Cole, G.; Hogan, J.; Aulton, M. E. Pharmaceutical coating technology; Taylor and Francis: London, 1995.